

Self-rotating 3D chiral mechanical metamaterials

K. K. Dudek^{1,2}, A. Drzewinski², and M. Kadic¹

¹Institut FEMTO-ST, CNRS, Université Bourgogne Franche-Comté, Besançon 25030, France

²Institute of Physics, University of Zielona Gora, ul. Szafrana 4a, 65-069 Zielona Gora, Poland

Abstract

In this work, we demonstrate that three-dimensional chiral mechanical metamaterials are able to self-twist and control their global rotation. We also discuss the possibility of adjusting the extent of the global rotation manifested by the system in a programmable manner. In addition, we show that the effect of the global rotation can be observed both for small systems composed of a single structural unit as well as more complex structures incorporating several structural elements connected to each other. Finally, it is discussed that the results presented in this work are very promising from the point of view of potential applications such as satellites or telescopes in space, where appropriately designed mechanical metamaterials could be used for the attitude control as well as other systems where the control of the rotational motion is required.

1 Introduction

Mechanical metamaterials [1, 2, 3, 4] are a class of novel materials that exhibit their effective properties due to their rational design rather than the chemical composition. Based on their structure, these systems can exhibit counterintuitive mechanical properties such as negative Poisson's ratio (auxetic behaviour) [1, 2, 5, 6, 7, 8, 9, 10, 11, 12, 13, 14], negative stiffness [15, 16, 17, 18, 19, 20] or negative compressibility [21, 22, 23, 24, 25]. In recent years, a continuous growth of the metamaterials research field led to their implementation in the case of superior biomedical [26, 27] and protective devices [28, 29]. A lot of attention has been also devoted to the search of new ways of controlling the deformation and resulting mechanical properties of such materials in a programmable manner. To this aim, researchers have incorporated a number of approaches including the use of elastic [30, 31, 32], magnetic and other interactions [33, 34, 19] which allow to control the response of the system in the case of a specific application.

Despite numerous directions of studies related to mechanical metamaterials, there are still different types of mechanical behaviour which remain to be discovered. A very promising example of a new type of behaviour which has been recently reported [35, 36] corresponds to the potential of mechanical metamaterials with the appropriate mass distribution to induce and control their own global rotational motion, i.e. the rotation of the entire system with respect to its centre of mass (see Concept section). It is important to note that this effect is very different from other types of commonly studied types of mechanical behaviour such as the rotation of materials' subunits [37] or twisting of the entire system [38, 39, 40, 41, 42] induced by the application of external forces. In terms of its origin, the concept of the self-induced global rotation of mechanical metamaterials was first proposed in the case of the so-called rotating square system with an uneven mass distribution [35]. More specifically, in this study, it was reported that the deformation of the structure corresponding to the rotation of its components having different masses may result in the generation of the non-zero net angular momentum (see Mass assignment subsection). This, in turn, leads to the global rotation of the entire system, which effect stems from the conservation of angular momentum. In another work [36], this concept was also confirmed experimentally for the same type of the system. It is also interesting to note that the basic principle of the self-induced global rotation is the same as in the case of the so-called reaction wheels [43, 44] which are commonly used in the case of satellites and other devices employed in space to ensure their attitude control. Thus, mechanical metamaterials manifesting this phenomenon may be potentially applied in similar applications related to the control of the rotational motion of satellites and telescopes where they could replace or significantly improve the efficiency of the currently used devices.

The concept of the self-induced global rotation of mechanical metamaterials is not limited to a specific geometry of the system. In fact, one can use an arbitrary type of a structure to achieve this effect given that its internal deformation would result in the non-zero net angular momentum. This particular observation was reported in the recent publication by Dudek *et al.* [45] where it was shown that this effect can be observed for a number of different structures composed of rigid rotating structural units where the appropriate selection of the structure and mass distribution allow to maximise the extent of the global rotation. Particularly interesting in this regard are chiral systems [46, 47, 48, 49, 50, 51] as they were reported [45] to be able to manifest a superior extent of the self-induced global rotation in comparison to other structures where different groups of subunits rotate in opposite directions. In another recent study [52], this observation was confirmed experimentally where it was also identified which of the two-dimensional chiral mechanical metamaterials can exhibit the largest extent of the global rotation. However, it is important to note that all of these studies related to the concept of the self-induced and self-controlled global

rotation of mechanical metamaterials were only focused on two-dimensional systems and similar studies have never been conducted for three-dimensional mechanical metamaterials.

In this work, we analyse a particular three-dimensional mechanical metamaterial with a non-uniform mass distribution in order to assess its potential to induce its own global rotational motion. An attempt will be made to verify whether the factors such as the variation in the mass distribution can be used to control the extent of this phenomenon. Finally, we will analyse the possibility of achieving such control in a programmable manner.

2 Concept

It is known that mechanical metamaterials can deform in an abundance of different ways depending on their design and the way how the external forces are being applied to them. However, such structures can also deform as a result of the application of internal forces, e.g. forces originating from elastic properties of structural elements. In the latter case, as reported in the recent studies [45, 52], the mechanical deformation can lead to the global rotation of the entire system with respect to its centre of mass. However, the observation of this effect is not possible for an arbitrary mechanical metamaterial. As explained in detail in [35, 36], in order for the self-induced global rotation to occur, the considered mechanical metamaterial must be designed in a way where the net angular momentum associated with all structural elements assumes the value different than zero as the structure is being deformed. Then, due to the conservation of angular momentum principle, the entire system must rotate with respect to its centre of mass in the direction opposite to that corresponding to the net angular momentum. As discussed in [35, 36], to design the structure in a manner enabling it to exhibit the self-induced global rotation one can consider a number of different approaches including a non-uniform mass distribution as is the case for the model proposed in this study. On the other hand, it is also worth to note that the considered effect of the self-induced global rotation can be also observed for structures other than mechanical metamaterials. One such example can be reaction wheels[43, 44] which based on the effect described above are capable of controlling the rotational motion of satellites.

3 Model

3.1 Geometry and interactions

In this work, we analyse a particular three-dimensional mechanical metamaterial that is shown schematically in Fig.1(a). We assume that the considered system consists of two identical in terms of their geometry hexagonal planes. These planes are constituted by points located at their vertices and centres where different points are connected to each other by means of rigid rods as shown schematically in Fig.1. It is also assumed that points within the system are assigned with different masses in a manner so that in the top layer of the structure there is one point having a mass m_1 and six points having a mass m_2 (see Fig. 1(a)). Similarly, in the bottom layer of the system, there is one point having a mass m_3 and the remaining six points are assigned the mass m_4 . Based on Fig. 1(a), one can also note that the linear dimension corresponding to hexagons formed by these points is denoted as l_a . Furthermore, the two adjacent hexagonal planes are connected to each other through rigid bonds having their length governed by the two-body harmonic potential. The equilibrium length of such bonds is denoted as l and due to their rigidity it remains approximately unchanged during the deformation process.

The deformation process of the considered system is induced by the bond connecting centres of the two hexagonal planes constituting the structure. The length of this bond is governed by the harmonic potential associated with the stiffness constant k_1 and the equilibrium length denoted as h_{eq} . At the beginning of the deformation process, the bond is assumed to be stretched so that its length is equal to h , where $h > h_{eq}$ (see Fig. 1(a)). Thus, there is a force originating from the presence of this spring-like bond that acts on both of the hexagonal planes constituting the system and in terms of magnitude is the same for both surfaces. However, it is important to note that the application of such forces does not result solely in the translational motion of the considered planes along the z -axis. More specifically, due to the presence of the oblique bonds, the translational motion is accompanied by the rotational motion of both of these surfaces with respect to their centres of mass.

In order to ensure that the behaviour of the system could represent the way how similar structures act in real life, it is assumed that its deformation corresponds to a certain resistance induced by bonded interactions between points constituting the system. More specifically, such resistance originates from three-body bonded interactions responsible for hinging between bonds connecting different pairs of points and four-body bonded interactions corresponding to the torsional motion within the structure (see Fig.1(c)). It should be also noted that the three-body bonded interactions grant the stability of the system and allow to ensure that the two hexagonal planes remain planar and parallel with respect to each other.

In terms of the mathematical formalism, bonds connecting different pairs of points which correspond to two-body bonded interactions have their length governed by the harmonic potential defined as $\frac{1}{2}k_1(l_i - l_{i,eq})^2$ where l_i and $l_{i,eq}$ represent the current and the equilibrium length of a specific i -th bond respectively. Similarly, the three-body bonded interactions are associated with the potential defined as $\frac{1}{2}k_2(\theta_{ijk} - \theta_{ijk,eq})^2$ where k_2 is a constant. Finally, the potential corresponding to four-body bonded interactions can be defined as $\frac{1}{2}k_3(\theta_{ijkl} - \theta_{ijkl,eq})^2$. In this case, the angle θ_{ijkl} corresponds to the angle between two vectors formed by pairs of points denoted as i, j and k, l as shown in

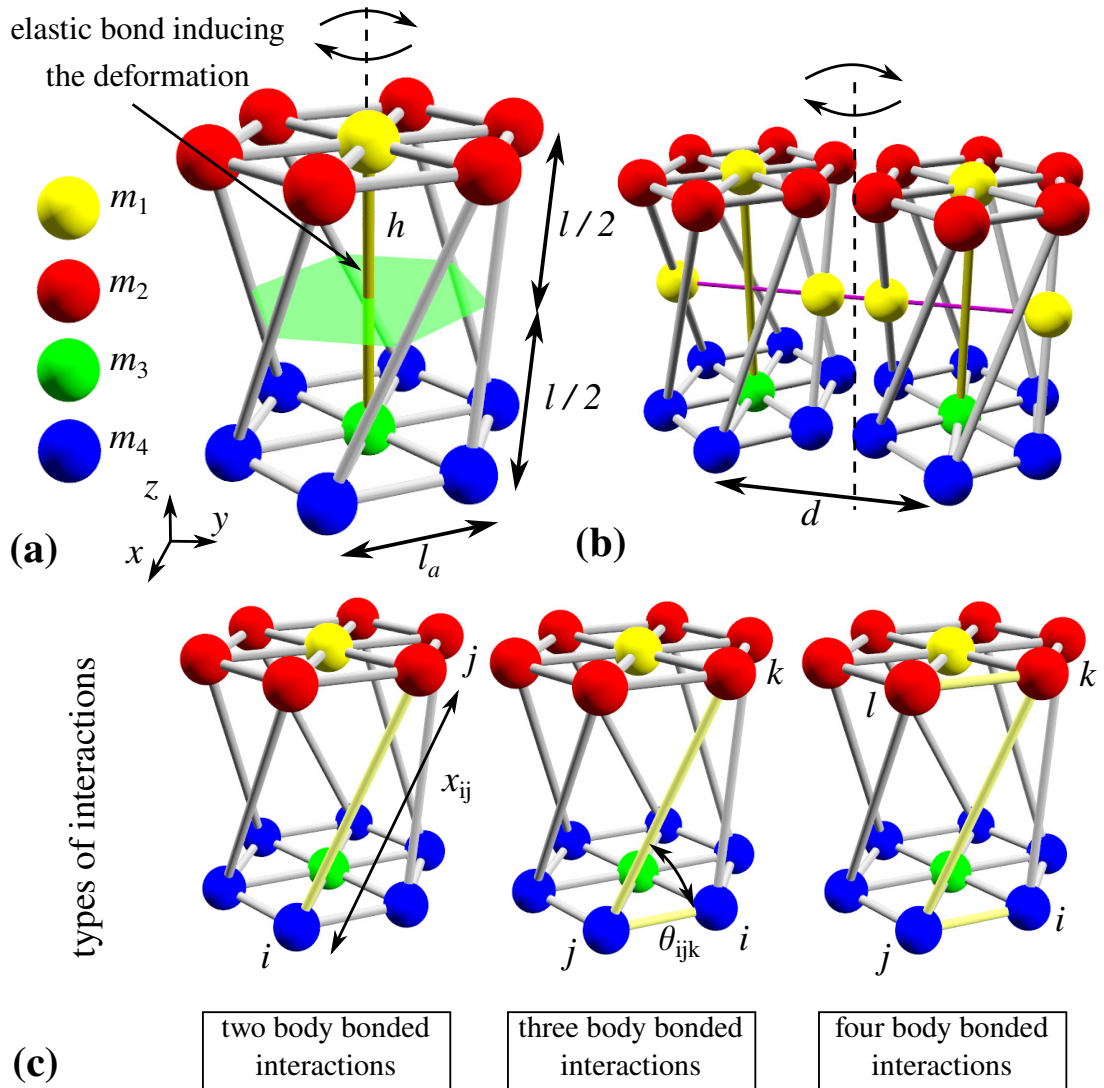


Figure 1: Panels show: (a) 3D graphical representation of the considered system having a potential to exhibit the global rotation with respect to the vertical axis parallel to the spring inducing the deformation of the system, (b) graphical representation of the second system analysed in this work which corresponds to two structures shown on panel (a) connected together by means of the purple rod-like bonds passing through centres of oblique ligaments. Panel (c) shows an example of how different interactions between points within the system are defined. The transparent hexagonal shape shown on panel (a) having its vertices defined by centres of a specific set of bonds within the system is used in order to determine the extent of the global rotation exhibited the structure during the deformation process.

Fig.1(c). It is also worth to note that in order to determine the force acting on points within the system as a result of the presence of bonded interactions listed above, it is sufficient to calculate the gradient of a given potential associated with a specific point with respect to its position vector.

3.2 Mass assignment

In order to observe the self-induced global rotation of a mechanical metamaterial it is necessary to construct it in a way so that the rotational motion of its constituents results in a non-zero net angular momentum. This in turn may prove to be difficult for certain systems and requires a very careful mass distribution. In the case of the considered model, the easiest method to achieve it seems to be the distribution of mass that allows both surfaces to exhibit translational motion at the same speed (in terms of magnitude). As a result, due to the presence of oblique bonds (see Fig.1), both planes would rotate with the same in terms of magnitude but directed in the opposite direction angular velocity. In such a case, if the planes were to have a different moment of inertia, then both of them would also have a different angular momentum. Thus, it would be possible to observe a non-zero net angular momentum which would have to be compensated by the angular momentum associated with the global rotation of the entire system in order to satisfy the conservation of angular momentum principle.

In the considered model, the two hexagonal planes constituting the system have a mass which can be described as $m_1 + 6m_2$ (top layer) and $m_3 + 6m_4$ (bottom layer). Thus, in order to satisfy the first of the aforementioned conditions corresponding to both planes moving vertically with the same in terms of magnitude but opposite speed,

$m_1 + 6m_2$ must be equal to $m_3 + 6m_4$. It is also worth to note that this condition is not required to observe the self-induced global rotation but significantly simplifies the analysis of the extent of this effect. Furthermore, in order to ensure that the moment of inertia of both planes is different, one can note that only masses denoted as m_2 and m_4 make a non-zero contribution to the moment of inertia of a given plane as masses m_1 and m_3 are defined on the axis of rotation. In other words, to potentially observe the effect of the self-induced global rotation, it is sufficient to ensure that $m_2 \neq m_4$. In view of this, in the further part of this work, the analysed results are generated for systems corresponding to $m_2/m_4 = 1, 2, 5$ where the mass of both planes is always the same and is equal to 0.5 kg.

3.3 Modeling and Parameters

The considered systems are analysed through the use of Molecular Dynamics (MD) simulations utilising the fourth order Runge-Kutta algorithm [53] for a constant time-step $\Delta t = 10^{-6}$ s. It is also assumed that there are not any external forces acting on the analysed structures. Thus, all forces acting on the system originate from bonded interactions. Furthermore, to generate the results presented in this study, different potentials governing the deformation mechanism are defined uniquely depending on the position of a given bond within the system. More specifically, upon taking two-body bonded interactions into consideration, the value of k_1 is set to be equal to 240 N/m in the case of the vertical bond inducing the deformation of the entire system. On the other hand, this constant is set to be equal to $2 \cdot 10^8$ N/m for bonds forming hexagonal planes (see Fig.1) as these planes are supposed to be rigid throughout the deformation. In addition to this, constant k_1 is set to be equal to $2 \cdot 10^9$ N/m for oblique bonds causing the rotation of hexagonal planes as the entire system is being deformed. Furthermore, it is assumed that the initial and equilibrium length of each of the two-body bonds was the same within the entire system with exception for the vertical bond as discussed above. More specifically, $h_{eq} = 0.18$ m, $h = 0.3$ m and $l_a = 0.2$ m.

Similarly to two-body bonded interactions, the constant k_2 associated with three-body bonded interactions is also set to assume different values depending on the position of a given bond within the system. For all of the three-body bonds like the one shown in Fig.1(c), k_2 is assumed to be equal to 2 J rad⁻². On the other hand, three-body bonds governed by the harmonic potential are also used between points forming hexagonal planes to ensure their rigidity should two-body bonds prove to be insufficient. In this case, $k_2 = 1$ J rad⁻². Such bonds are also used in order to ensure that both of the hexagonal planes remain parallel with respect to each other in which case k_2 assumes the value of 2000 J rad⁻². Finally, it is important to mention that within the system there is only one type of four-body bonds where all of the bonds are resembling the bond shown schematically in Fig.1(c). In this case, the value of k_3 used in the definition of the harmonic potential is equal to 0.5 J rad⁻². It is also important to emphasise the fact that the equilibrium angles related to all three-body and four-body bonds present within the system are matching the initial configuration of the system.

4 Results and discussion

In this work, in order to assess the possible extent of the self-induced global rotation of the system shown in Fig.1(a)(see Appendix A to find an information about the way how the extent of the global rotation is calculated), we analyse several variations of this structure with each of them having a different mass distribution. However, as discussed in more detail in the Model section, the top and the bottom plane of each of these systems have exactly the same mass which should make it possible to measure the extent of the self-induced global rotation in the aforementioned manner. Thus, before analysing the possibility of observing the considered phenomenon, it is important to first verify whether this condition related to both planes moving with the same in terms of magnitude but opposite speed is satisfied. Based on Fig. 2(b), one can note that for all of the considered systems corresponding to m_2/m_4 mass ratios equal to 1, 2 and 5, this behaviour can be indeed observed. More specifically, in all of these cases, the top and bottom plane of the specific structure move along the z -axis approximately with the same speed but in opposite directions. One can also note that for all of the considered cases, the extent of translation of the hexagonal planes is the same, i.e. $|\Delta h|$ reaches approximately the same maximum value for all configurations. The only difference corresponds to the fact that $|\Delta h|$ changes at a different rate for each mass arrangement. This in turn stems from the fact that the difference in the mass distribution results in a different moment of inertia associated with planes constituting each of the structures.

Based on Fig.2(c), one can note that the difference in the mass distribution results in a very different extent of the global rotation manifested by considered systems. In fact, for the first of the structures corresponding to $m_2/m_4 = 1$, there is no global rotation. This stems from the fact that in this particular case, both the top and bottom hexagonal planes have exactly the same moment of inertia. Hence, both planes have the same in terms of magnitude but opposite angular momentum and the structure cannot exhibit the global rotation as it would violate conservation laws. Furthermore, one can note that this is clearly not the case for structures where $m_2/m_4 = 2$ and 5. More specifically, in both of these cases, the non-zero global rotation can be observed where the maximum extent of this effect is approximately equal to 4.47° and 8.95° respectively (the graphical representation of the mechanical deformation of the system corresponding to the $m_2/m_4 = 5$ ratio is shown in Fig.2(d-e)). One can also note that in general, upon increasing the value of the m_2/m_4 ratio, it is possible to increase the extent of the global rotation. The reason for that is the fact that the larger the m_2/m_4 coefficient the larger the difference in the moment of inertia

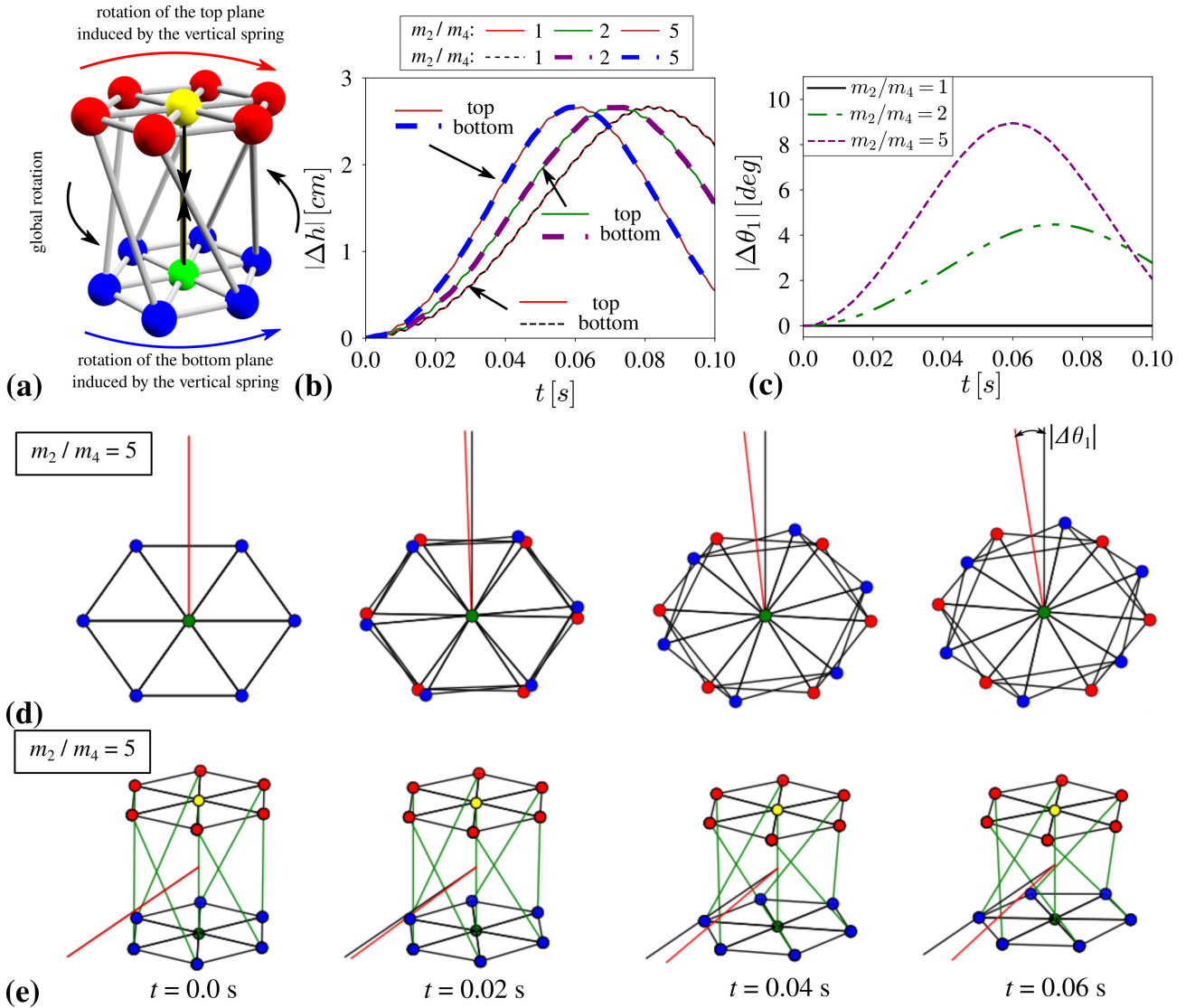


Figure 2: Panels show: (a) 3D diagram portraying the deformation mechanism leading to the global rotation, (b) the absolute value of the translation of the top and bottom layer of the system along the z -axis during the deformation process, (c) variation in the extent of the global rotation for different types of the mass distribution, (d) projection of the evolution of the system with $m_2/m_4 = 5$ in the xy plane and (e) the same process as on panel (d) portrayed in 3D. On panels (d) and (e) the auxiliary black and red solid lines indicate the initial and final orientation of the system respectively.

associated with the two hexagonal planes. Thus, due to the fact that they rotate with the same angular velocity, the net angular momentum which must be compensated by the global rotation becomes increased.

Upon having a closer look at the results provided in Fig.2(c) one can note that the direction of the manifested global rotation matches predictions that one should make based on the way how the model is defined. In other words, the direction of the global rotation is opposite to the direction of rotation of a heavier hexagonal plane corresponding to masses m_2 located at its vertices. This in turn is essential in order to satisfy the conservation of angular momentum principle. Furthermore, it is also possible to note that despite the fact that during the initial part of the deformation process the extent of the global rotation $|\Delta\theta_1|$ seems to be constantly increasing at one point this trend changes and $|\Delta\theta_1|$ starts decreasing for each system where $m_2/m_4 \neq 1$ (i.e. the system where all masses are the same). This stems from the fact that the deformation is induced by the elastic spring-like bond which must overcome a gradually growing resistance originating from different bonded interactions described in the Model section in order to deform the system. Thus, it is obvious that at certain point the system must start deforming back towards the initial configuration similarly to what would be the case for the initially stretched and released rubber band. At this point, it is also worth to note that in addition to the mass distribution, another factor that can affect the extent of the self-induced global rotation is the length of oblique ligaments (having the length l in Fig.1) and by extension, the height of the system h (see Appendix B).

After determining that it is possible for the system shown in Fig.1(a) to induce its own global rotational motion, it is also interesting to check whether such effect could be observed for larger structures which are composed of more than one structural unit. To do this, in this work, we analyse the behaviour of the structure shown in Fig.1(b) where

as discussed in the Model section, the only difference between this and the former system is the presence of two identical structural units instead of one where these structural units are connected to each other by means of the appropriately defined three-body interactions (see Fig.1(b)). In fact, the only reason to use such additional bonds, which are represented graphically by means of a purple rod in Fig.1(b), is to ensure that both cylindrical parts of the structure would rotate together should the internal interactions induce such motion.

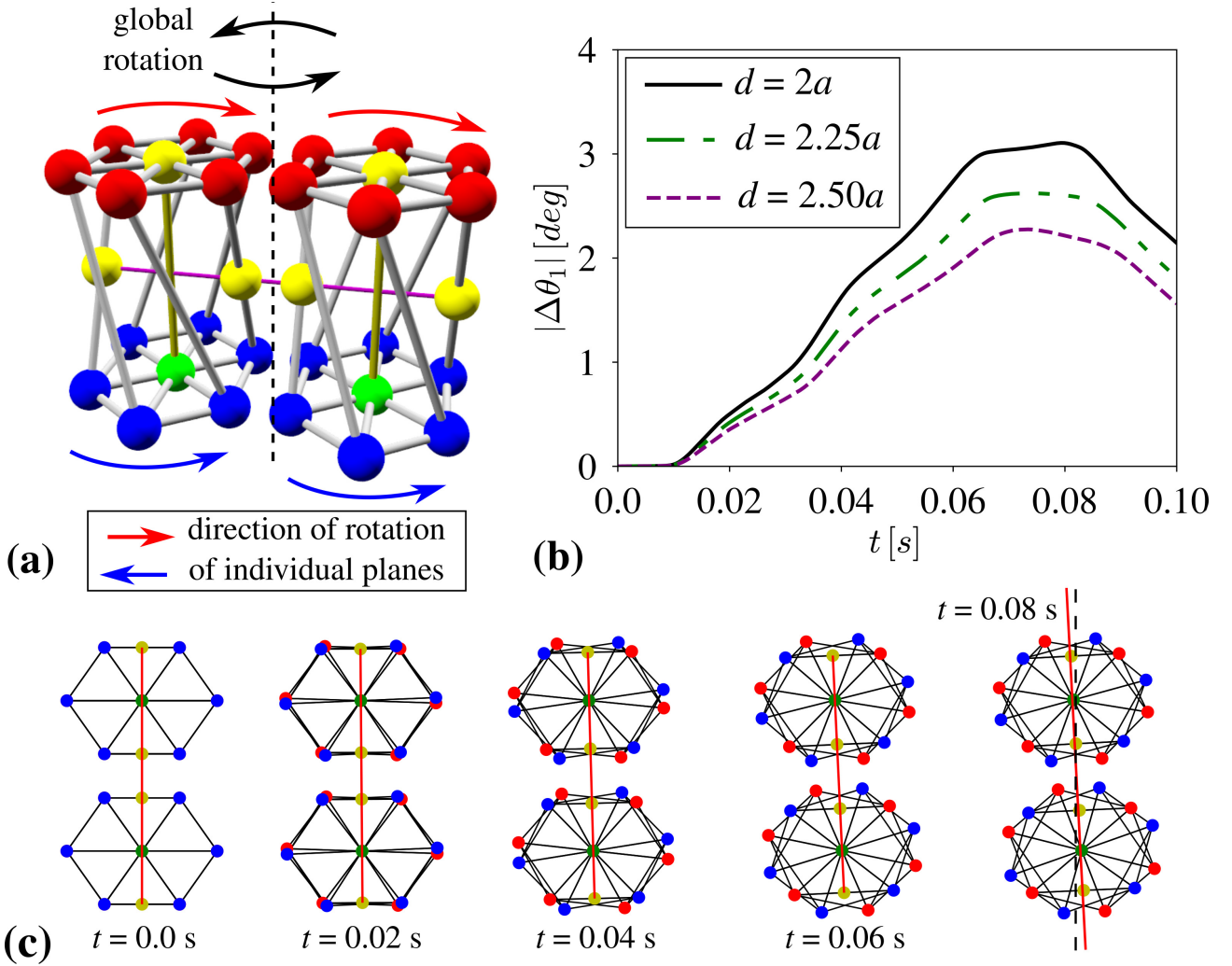


Figure 3: Panels: (a) diagram portraying different types of rotation induced during the deformation process, (b) variation in the extent of the global rotation for structures corresponding to a different separation distance d between centres of its structural elements and (c) graphical representation of the deformation of the system from the perspective of the projection in the xy plane. The black dashed auxiliary line represents the initial orientation of the undeformed system where the solid red lines defines the orientation of the system at the time when $\Delta\theta_1$ assumes the maximum value.

As shown in Fig.3(b), the deformation of the system portrayed in Fig.1(b) which consists of the two structural elements with the mass ratio $m_2/m_4 = 5$ leads to the global rotation of the entire system occurring with respect to its centre of mass. However, unlike in the case of the structure composed of only one structural unit, in this case, the centre of mass is not located within any of these structural elements. Instead, it is located between the structural units at the distance $d/2$ from their respective centres of mass (measured in the xy plane). One can also note that the direction of the manifested global rotation, which is graphically represented in Fig.3(c), is opposite to the direction of rotation of hexagonal planes associated with masses m_2 . This in turn, as discussed during the analysis of results presented in Fig.2, is in agreement with theoretical predictions.

In addition to the fact that the self-induced global rotation can be observed for the system shown in Fig.1(b) given the appropriate mass distribution, it is also important to analyse the extent of this effect. According to Fig.3(b), the maximum extent of the global rotation for the system composed of two structural units is significantly smaller than is the case for the structure consisting of one structural unit. More specifically, for the best performing of the analysed examples, the maximum extent of the global rotation is approximately equal to 3.12° which result is almost three times smaller than is the case for the system composed of one structural unit associated with the same mass distribution. Such a significant decrease in the extent of the global rotation in the case of the structure portrayed in Fig.3(a) stems from the fact that masses are moved significantly further away from the axis of global rotation in comparison to the system constituted by one structural unit. Hence, the corresponding moment of inertia related to

the global rotational motion is also significantly larger. Furthermore, one can note that upon increasing the value of the separation distance between the two structural units, the extent of the global rotation becomes gradually smaller. This behaviour, similarly to the previous observation, can be also explained by the fact that the increase in the value of d increases the moment of inertia associated with the global rotation.

At this point, it is important to note that there is one limitation of the considered model. Namely, each of the analysed systems can induce its global rotational motion only as long as it is deforming in a specific direction which process corresponds to the specific direction of rotation of its constituents. The change in the direction of the deformation process, e.g. the extension of the system after it was initially being compressed, would lead to the opposite direction of the global rotation. As a matter of fact, such behaviour is captured in Fig.2(c) and Fig.3(b) where once the structure starts deforming back towards the initial configuration, the system commences the rotation in the opposite direction to what was initially the case. It is also necessary to remember that in many real-life situations, we would want to have an opportunity to observe the global rotation to the desired (sometimes large) extent which is not limited by geometric constraints. This can be achieved should one for example incorporate magnets and electromagnets in the analysed system in a manner shown schematically in Fig.4. More specifically, in the case of the structure with mobile magnets being able to slide along rigid bars as shown in Fig.4, it is possible to conveniently make the moment of inertia of the two hexagonal planes to be different by adjusting magnets' positions along such bars in a programmable manner. This can be done by means of the appropriately located electromagnets that can either repel or attract unconstrained magnets up to the point where they would assume an expected position along the bar. Thus, during the deformation process, the two hexagonal planes having a significantly different moment of inertia could generate the non-zero net angular momentum which would lead to the global rotation. In addition to this, should the system stop deforming in a specific direction due to reaching its geometric limit, positions of sliding magnets could be changed. Then, upon reversing the moment of inertia of the two hexagonal planes by changing the type of interaction between magnetic inclusions, it would be possible to continue the global rotation in the same direction as was the case before reaching the geometric constraint even though the direction of the mechanical deformation would be reversed. This way, in theory, it would be possible to attain an arbitrary angle of the global rotation. Finally, it is very important to emphasise the fact that the condition proposed in this study related to the rigidity of rods constituting the system is very significant. This stems from the fact that if this condition was not satisfied, the rods constituting the system would be prone to buckle during the deformation process which would likely minimise the extent of rotation of the hexagonal planes constituting the system and by extension would result in the negligible extent of the global rotation.

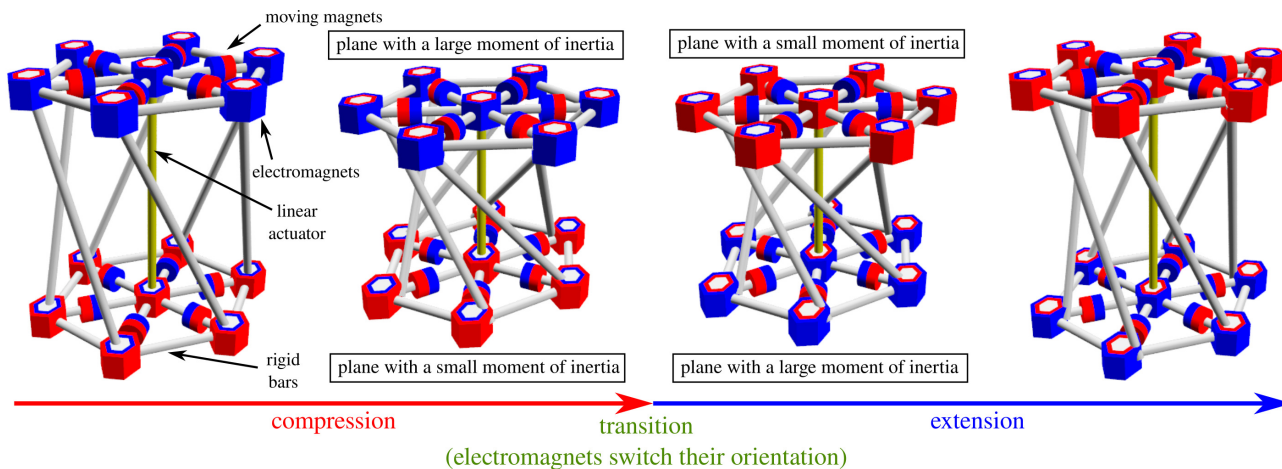


Figure 4: Diagram showing the concept of the system with fixed electromagnets and magnets moving along rigid bars. In this case, mobile magnets may move either towards the outer or central electromagnets depending on their mutual orientation. The global rotation corresponding to the depicted deformation process is not presented for the sake of the clarity.

All of this is very important as in this work it is shown that the considered 3D mechanical metamaterial can induce its own global rotational motion. It is also discussed that the extent of the global rotation can be controlled via the variation in the mass distribution within the system. In addition to this, it is discussed how the system considered in this study can be modified in order to make it possible to observe the self-induced global rotation to an arbitrary extent (see Fig.4). Furthermore, it is also shown that the effect studied in this work is not limited only to one structural unit and can be extended to larger structures incorporating a number of such structural elements connected together (see Fig.3). All of these results offer several advantages in comparison to two-dimensional mechanical metamaterials that had been studied from the point of view of the considered phenomenon. First of all, the considered 3D structures do not need to change the surface of rotating planes constituting the structure during the deformation process. This in turn could prove to be very important in the case of applications such as the control over the rotational motion of the satellite or other object employed in space where available space is very limited. Furthermore, the extent of the self-induced global rotation of the 3D structures can be relatively large in comparison to a majority of two-dimensional systems upon comparing a single deformation cycle. All of these features make the systems discussed in this work to

be suitable to be implemented in the case of a variety of applications including satellites and telescopes employed in space. They can also prove to be very useful in the design of novel robots which could utilise the concept proposed in this work to improve their mobility.

5 Conclusion

In this work, it is shown that three-dimensional mechanical metamaterials can induce their own global rotational motion. It is also shown that the extent of such rotation can be controlled via the variation in the mass distribution within the system. Furthermore, it is discussed that such control over the rotational motion of the structure can be potentially achieved in the programmable manner should one for example decide to utilise appropriately located magnetic inclusions. In addition to this, it is discussed that the concept of the self-induced global rotation can be observed both for small structures composed of a single structural unit as well as larger systems incorporating several structural elements. All of these results are very promising from the point of view of a variety of applications as they indicate that the concept presented in this work could be used in the case of satellites, telescopes employed in space and many others devices that require the control over their rotational motion.

Data

This article has no additional data

Contributions

K.K.D. coined the concept, proposed the methodology, generated the main results and wrote the first version of the manuscript. A.D. and M.K. helped with writing of the manuscript and the supervision of the project. All authors reviewed the manuscript and contributed to the discussion.

Competing interests

The authors have no competing interests.

Funding

K.K.D. and A.D. acknowledge the financial support from the program of the Polish Ministry of Science and Higher Education under the name "Regional Initiative of Excellence" in 2019 - 2022, project no. 003/RID/2018/19, funding amount 11 936 596.10 PLN. K.K.D. acknowledges the support of the Polish National Science Centre (NCN) in the form of the programme MINIATURA4, project No. 2020/04/X/ST5/00663 under the name "Programmable hierarchical mechanical metamaterials".

Appendix A: Calculation of the extent of the global rotation

In this work, we analyse two systems shown in Fig.1(a) and Fig.1(b). It is possible to note that while discussing the geometry of the system, we only focused on the structure shown in Fig.1(a) as the system presented in Fig.1(b) is almost identical. More specifically, it consists of two structures like the one shown in Fig.1(a) which are connected to each other by means of the additional rod passing through centres of oblique ligaments as shown in Fig.1(b).

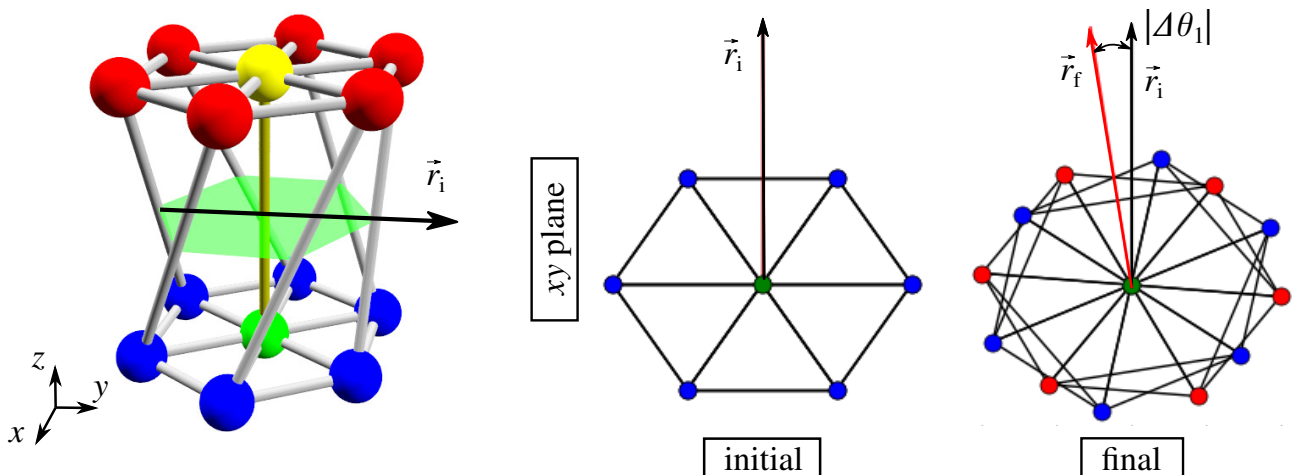


Figure A1: The diagram showing how the extent of the global rotation was calculated for the system composed of a single structural cell.

For the systems shown in Fig.1(a), the extent of the global rotation is evaluated by means of the rotation of the auxiliary hexagonal plane which is marked by the light green colour. The vertices of this auxiliary plane correspond to centres of oblique ligaments. Furthermore, due to the fact that both, the top and bottom surface of the structure move with the same in terms of magnitude but opposite velocity and angular velocity, positions of centres of oblique bonds would be fixed in space if the system does not exhibit a global rotational motion. This means that the extent of the global rotation can be also interpreted as a net rotation of the top and bottom plane of the system. This stems from the fact that if there was no global rotation, then the combination of the rotation of the top and bottom planes would be equal to zero. Thus, as shown in Fig. A1, if one was to define the initial orientation (in the xy plane) of the aforementioned green hexagonal surface by means of the vector \vec{r}_i and its final orientation as the vector \vec{r}_f (once the system is deformed), then the extent of the global rotation could be calculated by means of the following expression: $|\Delta\theta_1| = \arccos\left(\frac{\vec{r}_i \cdot \vec{r}_f}{|\vec{r}_i||\vec{r}_f|}\right)$. However, at this point it is also important to emphasise the fact that should one consider the system where top and bottom planes have different masses then the approach described above could not be implemented.

The second system considered in this work (see Fig.1(b)) exhibits the global rotation in a very different manner than is the case for the structure shown in Fig.1(a). This stems from the fact that for the first structure, it is easy to confuse the extent of the global rotation with rotation of individual planes as both of these rotational motions occur with respect to the same axis. However, for the second analysed system, it is very simple to identify the global rotation manifested by the structure as it occurs with respect to the vertical axis located between the two structural elements constituting the system (see Fig.1(b)). More specifically, one can determine it by means of the extent of rotation of an auxiliary vector connecting centres of two topmost (or bottommost) hexagonal surfaces measured in the xy plane. Finally, it should be noted that for all of the structures considered in this work, the global rotation will be denoted as $\Delta\theta_1$.

Appendix B: Parametric analysis of the behaviour of the single-cell structure

At this point, it is also worth to note that in addition to the mass distribution, another factor that can affect the extent of the self-induced global rotation is the length of oblique ligaments (having the length l in Fig.1) and by extension, the height of the system h . In Fig. B1 (a), it is shown that for relatively small extents of the mechanical deformation, structures corresponding to the relatively large value of h can exhibit a slightly larger extent of the global rotation than their shorter counterparts. On the other hand, very tall structures (large value of h) correspond to oblique ligaments having an almost vertical orientation which from the practical point of view makes it difficult to induce the deformation. Furthermore, for such structures, it would be difficult to retain the rigidity of oblique ligaments which is essential to observe the considered effect. Of course, this does not mean that from the point of view of future prototypes one should consider structures corresponding to very small values of h . This stems from the fact that the extent of the global rotation of such systems would be insignificant as the mechanical deformation corresponding to the compression of the system along the z -axis (vertical dimension) would result in the very small magnitude of rotation of the two hexagonal planes constituting the system.

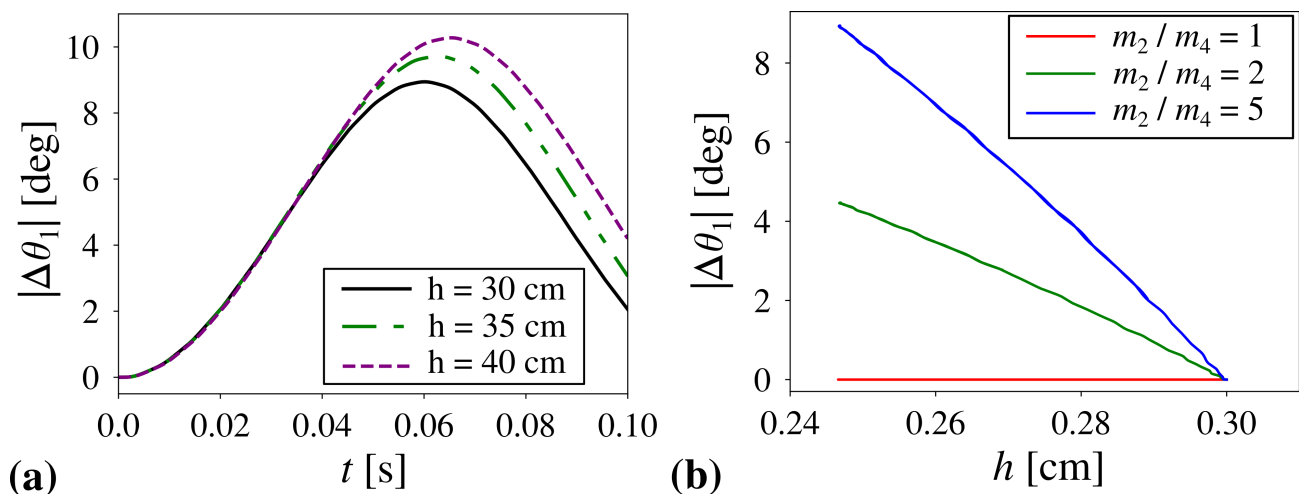


Figure B1: Panels show: a) the variation in the extent of the global rotation for systems corresponding to a different initial height h and b) the change in the extent of the global rotation plotted against the corresponding change in the height of the structure for systems associated with different values of the mass ratio m_2/m_4 . All results shown on panel (a) were generated for the same mass ratio $m_2/m_4 = 5$.

In the main text, in Fig. 2(c), it is shown how does the extent of the global rotation change in time for different

types of the mass distribution. In addition, in Fig. 2(b), it is presented how does the height of the system change for each of the deformation processes portrayed in Fig. 2(c). However, it would be very interesting to combine these two graphs in order to show quantitatively how does the extent of the global rotation change with respect to the extent of the vertical compression measured along the z -axis (change in h). This result is provided in Fig.B1(b), where it is shown that for the similar extent of the mechanical compression along the z -axis, the largest extent of the global rotation can be observed for the structure with the largest m_2/m_4 mass ratio as expected based on the discussion included in the main text.

References

- [1] Lakes R. 1987 Foam structures with a negative Poisson's ratio. *Science* **235**, 1038-1040.
- [2] Wojciechowski KW. 1989 Two-dimensional isotropic system with a negative poisson ratio. *Phys. Lett. A* **137**, 60-64.
- [3] Barchiesi E, Spagnuolo M, Placidi L. 2019 Mechanical metamaterials: a state of the art. *Math. Mech. Solids* **24**, 212-234.
- [4] Ma G, Fu C, Wang G, del Hougne P, Christensen J, Lai Y, Sheng P. 2016 Polarization bandgaps and fluid-like elasticity in fully solid elastic metamaterials. *Nat. Commun.* **7**, 13536.
- [5] Evans KE, Nkansah MA, Hutchinson IJ, Rogers SC. 1991 Molecular network design. *Nature* **353**, 124.
- [6] Milton GW. 1992 Composite materials with poisson's ratios close to -1. *J. Mech. Phys. Solids* **40**, 1105-1137.
- [7] Babae S, Shim J, Weaver JC, Chen ER, Patel N, Bertoldi K. 2013 3D Soft Metamaterials with Negative Poisson's Ratio. *Adv. Mater.* **25**, 5044-5049.
- [8] Lim T-C. 2019 A class of shape-shifting composite metamaterial honeycomb structures with thermally-adaptive Poisson's ratio signs. *Compos. Struct.* **226**, 111256.
- [9] Hunt GW., Dodwell TJ. 2019 Complexity in phase transforming pin-jointed auxetic lattices. *Proc. R. Soc. A* **475**, 20180720.
- [10] Rayneau-Kirkhope D, Zhang C, Theran L, Dias MA. 2019 Analytic analysis of auxetic metamaterials through analogy with rigid link systems. *Proc. R. Soc. A* **474**, 20170753.
- [11] Lim T-C. 2020 Maximum Stresses in Rectangular Auxetic Membranes. *Phys. Status Solidi B*, 2000300.
- [12] Tretiakov KV, Wojciechowski KW. 2020 Auxetic, Partially Auxetic, and Nonauxetic Behaviour in 2D Crystals of Hard Cyclic Tetramers. *Phys. Status Solidi RRL* **14**, 2000198.
- [13] Crespo J, Duncan O, Alderson A, Montáns FJ. 2020 Auxetic orthotropic materials: Numerical determination of a phenomenological spline-based stored density energy and its implementation for finite element analysis. *Comput. Methods Appl. Mech. Eng.* **371**, 113300.
- [14] Cabras L, Brun M. 2014 Auxetic two-dimensional lattices with Poisson's ratio arbitrarily close to -1. *Proc. R. Soc. A* **470**, 20140538.
- [15] Lakes RS, Drugan WJ. 2002 Dramatically stiffer elastic composite materials due to a negative stiffness phase? *J. Mech. Phys. Solids* **50**, 979-1009.
- [16] Wang YC, Lakes RS. 2004 Extreme stiffness systems due to negative stiffness elements. *Am. J. Phys.* **72**, 40-50.
- [17] Florijn B, Coulais C, van Hecke M. 2014 Programmable mechanical metamaterials. *Phys. Rev. Lett.* **113**, 175503.
- [18] Hewage TAM, Alderson KL, Alderson A, Scarpa F. 2016 Double-negative mechanical metamaterials displaying simultaneous negative stiffness and negative Poisson's ratio properties. *Adv. Mater.* **28**, 10323.
- [19] Dudek KK, Gatt R, Grima JN. 2020 3D composite metamaterial with magnetic inclusions exhibiting negative stiffness and auxetic behaviour. *Mater. Des.* **187**, 108403.
- [20] Wang J, Nartey MA, Luo Y, Wang H, Scarpa F, Peng H-X. 2020 Designing multi-stable structures with enhanced designability and deformability by introducing transition elements. *Compos. Struct.* **233**, 111580.
- [21] Lakes R, Wojciechowski KW. 2008 Negative compressibility, negative Poisson's ratio, and stability. *Phys. Status Solidi B* **245**, 545-551.

- [22] Nicolaou ZG, Motter AE. 2012 Mechanical metamaterials with negative compressibility transitions. *Nat. Mater.* **11**, 608-613.
- [23] Lim T-C. 2017 2D structures exhibiting negative area compressibility. *Phys. Status Solidi B* **254**, 1600682.
- [24] Qu J, Kadic M, Wegener M. 2017 Poroelastic metamaterials with negative effective static compressibility. *Appl. Phys. Lett.* **110**, 171901.
- [25] Dudek KK, Attard D, Gatt R, Grima-Cornish JN, Grima JN. 2020 The Multidirectional Auxeticity and Negative Linear Compressibility of a 3D Mechanical Metamaterial. *Materials* **13**, 2193.
- [26] Zadpoor AA. 2017 Design for Additive Bio-Manufacturing: From Patient-Specific Medical Devices to Rationally Designed Meta-Biomaterials. *Int. J. Mol. Sci* **18**, 1607.
- [27] Kolken HMA, Janbaz S, Leeftang SMA., Lietaert K, Weinans HH, Zadpoor AA. 2018 Rationally designed meta-implants: a combination of auxetic and conventional meta-biomaterials. *Mater. Horiz.* **5**, 28-35.
- [28] Chan N, Evans KE. 1998 Indentation resilience of conventional and auxetic foams. *J. Cell. Plast.* **34**, 231-260.
- [29] Imbalzano G, Tran P, Ngo TD, Lee PVS. 2017 Three-dimensional modelling of auxetic sandwich panels for localised impact resistance. *J. Sandw. Struct. Mater* **19**, 291-316.
- [30] Schittny R, Bückmann T, Kadic M, Wegener M. 2013 Elastic measurements on macroscopic three-dimensional pentamode metamaterials. *Appl. Phys. Lett.* **103**, 231905.
- [31] Bertoldi K, Vitelli V, Christensen J, van Hecke M. 2017 Flexible mechanical metamaterials. *Nat. Rev. Mater.* **2**, 17066.
- [32] Mizzi L, Salvati E., Spaggiari A, Tan JC, Korsunsky AM. 2020 Highly stretchable two-dimensional auxetic metamaterial sheets fabricated via direct-laser cutting. *Int. J. Mech. Sci.* **167**, 105242.
- [33] Grima JN, Caruana-Gauci R, Dudek MR, Wojciechowski KW, Gatt R. 2013 Smart metamaterials with tunable auxetic and other properties. *Smart Mater. Struct.* **22**, 084016.
- [34] Schaeffer M, Ruzzene M. 2015 Wave propagation in reconfigurable magneto-elastic kagome lattice structures. *J. Appl. Phys.* **117**, 194903.
- [35] Dudek KK, Gatt R, Mizzi L, Dudek MR, Attard D, Grima JN. 2017 Global rotation of mechanical metamaterials induced by their internal deformation. *AIP Adv.* **7**, 095121.
- [36] Dudek KK, Wojciechowski KW, Dudek MR, Mizzi L, Grima JN. 2018 Potential of mechanical metamaterials to induce their own global rotational motion *Smart Mater. Struct.* **27**, 055007.
- [37] Gatt R, Mizzi L, Azzopardi JI, Azzopardi KM, Attard D, Casha A, Briffa J, Grima JN. 2015 Hierarchical Auxetic Mechanical Metamaterials. *Sci. Rep.* **5**, 8395.
- [38] Frenzel T, Kadic M, Wegener M. 2017 Three-dimensional mechanical metamaterials with a twist. *Science* **358**, 1072-1074.
- [39] Wu W, Geng L, Niu Y, Qi D, Cui X, Fang D. 2018 Compression twist deformation of novel tetrachiral architected cylindrical tube inspired by towel gourd tendrils *Extreme Mech. Lett.* **20**, 104-111.
- [40] Zhai Z, Wang Y, Jiang H. 2018 Origami-inspired, on-demand deployable and collapsible mechanical metamaterials with tunable stiffness. *Proc. Natl. Acad. Sci. U.S.A.* **115**, 2032-2037.
- [41] Vangelatos Z, Gu GX, Grigoropoulos CP. 2019 Architected metamaterials with tailored 3D buckling mechanisms at the microscale. *Extreme Mech. Lett.* **33**, 100580.
- [42] Farrugia P-S, Gatt R, Grima JN. 2020 The Push Drill Mechanism as a Novel Method to Create 3D Mechanical Metamaterial Structures. *Phys. Status Solidi RRL* **14**, 2000125.
- [43] Jin J, Ko S, Ryoo C-K. 2008 Fault tolerant control for satellites with four reaction wheels. *Control Eng. Pract.* **16**, 1250-1258.
- [44] Ismail Z, Varatharajoo R. 2010 A study of reaction wheel configurations for a 3-axis satellite attitude control. *Adv. Space Res.* **45**, 750-759.
- [45] Dudek KK, Gatt R, Wojciechowski KW, Grima JN. 2020 Self-induced global rotation of chiral and other mechanical metamaterials. *Int. J. Solids Struct.* **191-192**, 212-219.

- [46] Alderson A, Alderson KL, Attard D, Evans KE, Gatt R, Grima JN, Miller W, Ravirala N, Smith CW, Zied K. 2010 Elastic constants of 3-, 4- and 6-connected chiral and anti-chiral honeycombs subject to uniaxial in-plane loading. *Compos. Sci. Technol.* **70**, 1042-1048.
- [47] Wang Z, Jing L, Yao K, Yang Y, Zheng B, Soukoulis CM, Chen H, Liu Y. 2017 Origami-Based Reconfigurable Metamaterials for Tunable Chirality. *Adv. Mater.* **29**, 1700412.
- [48] Fernandez-Corbaton I, Rockstuhl C, Ziemke P, Gumbsch P, Albiez A, Schwaiger R, Frenzel T, Kadic M, Wegener M. 2019 New Twists of 3D Chiral Metamaterials. *Adv. Mater.* **31**, 1807742.
- [49] Wu W, Hu W, Qian G, Liao H, Xu X, Berto F. 2019 Mechanical design and multifunctional applications of chiral mechanical metamaterials: A review. *Mater. Des.* **180**, 107950.
- [50] Kadic M, Diatta A, Frenzel T, Guenneau S, Wegener M. 2019 Static chiral Willis continuum mechanics for three-dimensional chiral mechanical metamaterials. *Phys. Rev. B* **99**, 214101.
- [51] Chen Y, Kadic M, Guenneau S, Wegener M. 2020 Isotropic Chiral Acoustic Phonons in 3D Quasicrystalline Metamaterials. *Phys. Rev. Lett.* **124**, 235502.
- [52] Dudek KK. 2020 New type of rotation of chiral mechanical metamaterials. *Smart Mater. Struct.* **29**, 115027.
- [53] Burden RL, Faires J.D., 1985. Numerical Analysis. PWS.